http://doi.org/10.1093/plphys/kiab600 PLANT PHYSIOLOGY 2022: 188: 2308–2324

Plant Physiology®

Research Article

Antagonistic modules regulate photosynthesis-associated nuclear genes via GOLDEN2-LIKE transcription factors

Mengping Li ,[1,2] Keun Pyo Lee ,[1] Tong Liu,[1,2] Vivek Dogra ,[1,‡] Jianli Duan ,[1] Mengshuang Li,[1,2] Weiman Xing[1] and Chanhong Kim [1,*,†]

1 Shanghai Center for Plant Stress Biology, CAS Center for Excellence in Molecular Plant Sciences, Chinese Academy of Sciences, Shanghai, 200032, China
2 University of the Chinese Academy of Sciences, Beijing, 100049, China

*Author for correspondence: chanhongkim@cemps.ac.cn
†Senior author.
‡Present address: Division of Biotechnology, CSIR-Institute of Himalayan Bioresource Technology, Palampur, 176061, India

These authors contributed equally (M.L. and K.P.L.).

C.K. conceived the original screening and research plans. M.L., K.P.L., T.L., V.D., W.X., and C.K. designed the experiments. M.L., K.P.L., T.L., V.D., J.D., and M.S.L. performed the experiments. M.L., K.P.L., T.L., V.D., W.X., and C.K. analyzed the data. C.K. wrote the manuscript with significant contributions from M.L. and K.P.L. All authors discussed the results and reviewed the manuscript.

The author responsible for distribution of materials integral to the findings presented in this article in accordance with the policy described in the Instructions for Authors (https://academic.oup.com/plphys/pages/general-instructions) is: Chanhong Kim (chanhongkim@cemps.ac.cn).

Abstract

GOLDEN2-LIKE (GLK) transcription factors drive the expression of photosynthesis-associated nuclear genes (PhANGs) indispensable for chloroplast biogenesis. Salicylic acid (SA)-induced SIGMA FACTOR-BINDING PROTEIN 1 (SIB1), a transcription coregulator and positive regulator of cell death, interacts with GLK1 and GLK2 to reinforce the expression of PhANGs, leading to photoinhibition of photosystem II and singlet oxygen ($^1O_2$) burst in chloroplasts. $^1O_2$ then contributes to SA-induced cell death via EXECUTER 1 (EX1; $^1O_2$ sensor protein)-mediated retrograde signaling upon reaching a critical level. This earlier finding has initiated research on the potential role of GLK1/2 and EX1 in SA signaling. Consistent with this view, we reveal that LESION-SIMULATING DISEASE 1 (LSD1), a transcription coregulator and negative regulator of SA-primed cell death, interacts with GLK1/2 to repress their activities in Arabidopsis (*Arabidopsis thaliana*). Overexpression of LSD1 repressed GLK target genes, including PhANGs, whereas loss of LSD1 enhanced their expression. Remarkably, LSD1 overexpression inhibited chloroplast biogenesis, resembling the characteristic *glk1glk2* double mutant phenotype. Subsequent chromatin immunoprecipitation coupled with expression analyses further revealed that LSD1 inhibits the DNA-binding activity of GLK1 toward its target promoters. SA-induced nuclear-targeted SIB1 proteins appeared to interrupt the LSD1–GLK interaction, and the subsequent SIB1–GLK interaction activated EX1-mediated $^1O_2$ signaling, elucidating antagonistic modules SIB1 and LSD1 in the regulation of GLK activity. Taken together, we provide a working model that SIB1 and LSD1, mutually exclusive SA-signaling components, antagonistically regulate GLK1/2 to fine-tune the expression of PhANGs, thereby modulating $^1O_2$ homeostasis and related stress responses.

Received November 24, 2021. Accepted November 24, 2021. Advance access publication December 24, 2021

Introduction

Chloroplasts communicate with the nucleus via retrograde signaling (RS) in response to the ever-changing environment. Upon exposure to unfavorable environmental conditions, chloroplasts downregulate photosynthesis-associated nuclear genes (PhANGs), referred to as biogenic RS, but stimulate the expression of stress-related genes via alternate RS pathways, collectively called operational RS (Pogson et al., 2008; Li and Kim, 2021). The nuclear-encoded chloroplast GENOMES-UNCOUPLED 1 (GUN1) protein plays a pivotal role in the biogenic RS (Nott et al., 2006). GUN1 integrates various retrograde signals released by the disturbance in plastid gene expression, redox homeostasis, and tetrapyrrole biosynthesis in chloroplasts (Nott et al., 2006; Koussevitzky et al., 2007; CHan et al., 2016). Recent efforts also demonstrated that GUN1 functions in protein import (Wu et al., 2019), RNA editing (Zhao et al., 2019), protein homeostasis (Tadini et al., 2020), and tetrapyrrole synthesis in chloroplasts (Shimizu et al., 2019), which modulates the downstream RS. The well-known targets of GUN1-mediated RS are two nuclear genes encoding the GOLDEN2-LIKE (GLK) transcription factors (TFs), mainly implicated in the positive regulation of PhANGs and thus chloroplast biogenesis (Waters et al., 2009; Martin et al., 2016). When chloroplast functions are perturbated, as mentioned above, GUN1-mediated RS represses *GLK* transcription, thereby decelerating photosynthesis. In Arabidopsis (*Arabidopsis thaliana*), GLK1 and GLK2 function redundantly to express PhANGs, so the loss of both GLKs substantially impairs chloroplast biogenesis (Fitter et al., 2002).

Whereas GUN1 is known to participate in biogenic RS, the nuclear-encoded chloroplast EXECUTER 1 (EX1) protein participates in operational RS when chloroplasts produce a critical level of highly reactive singlet oxygen ($^1O_2$), primarily generated by the free tetrapyrrole molecules (potent photosensitizers; Wagner et al., 2004; Dogra et al., 2019). The Arabidopsis *fluorescent* (*flu*) mutant was initially utilized to explore a signaling role of $^1O_2$ since the *flu* mutant noninvasively and conditionally generates $^1O_2$ in chloroplasts upon a dark-to-light shift, which leads to cell death in young seedlings and growth inhibition in mature plants (Meskauskiene et al., 2001). Given that FLU protein represses tetrapyrrole synthesis in the Mg^{2+} branch in the dark, *flu* mutant overaccumulates free protochlorophyllide (Pchlide; a precursor of chlorophyllide) in the dark, which upon absorption of light energy generates $^1O_2$ by transferring the absorbed energy to the ground state of oxygen molecules (Meskauskiene et al., 2001; Apel and Hirt, 2004; Dogra et al., 2018). Later, the same group highlighted the role of FLU protein in the chlorophyll homeostasis under light conditions (Goslings et al., 2004), indicating that FLU protein functions as a negative regulator of Mg^{2+}-tetrapyrroles in both dark and light conditions. The subsequent forward genetic screen aimed to find the suppressor of *flu* and revealed EX1 as a key mediator of $^1O_2$-triggered nucleus-to-chloroplast signaling that primes $^1O_2$-dependent plant stress responses (Wagner et al., 2004; Lee et al., 2007). Nevertheless, although GUN1 and EX1 proteins are critical mediators for biogenic and operational RS and two events must be intertwined timely, the possible interplay between GUN1 and EX1 and crosstalk of their downstream signaling cascades remain unexplored. Moreover, multiple lines of evidence demonstrate that GUN1 is required for plant stress responses (Miller et al., 2007; Cheng et al., 2011; Zhang et al., 2011, 2013; Tang et al., 2014), proposing that its downstream target GLK1/2 may participate in chloroplast-mediated stress responses.

We lately demonstrated that the nuclear-targeted SIGMA FACTOR-BINDING PROTEIN 1 (SIB1), a defense-related transcription coregulator, interacts with GLK1/2 in response to an increase in foliar salicylic acid (SA; Lai et al., 2011; Lv et al., 2019). In the Arabidopsis *lesion-simulating disease 1* (*lsd1*) mutant grown under continuous light (CL) conditions, the transiently increased level of SA rapidly induces the otherwise undetectable SIB1, leading to its accumulation in both the nucleus and the chloroplasts (Lai et al., 2011; Lv et al., 2019). It is important to note that extended day length is one of the lesion-triggering external factors evoking SA-dependent runaway (uncontrolled) cell death (RCD) in the *lsd1* mutant (Dietrich et al., 1994; Lv et al., 2019). The SA receptor NONEXPRESSER OF PR GENES 1 (NPR1) induces the expression of *SIB1* and the dual targeting of SIB1 also occurs in wild-type (WT) plants after SA treatment (Xie et al., 2010; Lai et al., 2011; Lv et al., 2019). Whereas the loss of NPR1 abolishes *lsd1* RCD, the loss of SIB1 significantly delays RCD (Aviv et al., 2002; Lv et al., 2019), indicating that SIB1 is one of the RCD-triggering components directed by NPR1. Remarkably, the SIB1–GLK interaction in the nucleus enhances the expression of PhANGs, while chloroplast-localized SIB1 (cpSIB1) represses the expression of photosynthesis-associated plastid genes (PhAPGs; Morikawa et al., 2002; Lv et al., 2019). This concurrent uncoupled expression of PhANGs and PhAPGs increases $^1O_2$ levels in chloroplasts through enhanced photoinhibition in photosystem II (PSII; Lv et al., 2019). EX1, a $^1O_2$ sensor protein (Dogra et al., 2019), then mediates $^1O_2$-triggered RS to contribute to stress responses in *lsd1* mutant plants (Lv et al., 2019). It appears that SIB1 undergoes co-translational N-terminal acetylation (NTA) and posttranslational ubiquitination (Li et al., 2020). While NTA renders the nuclear SIB1 (nuSIB1) more stable, the latter modification promotes its turnover via the ubiquitin–proteasome system (UPS). The interplay of NTA and UPS seems to regulate nuSIB1-mediated stress responses finely. Nonetheless, earlier reports that nuSIB1–GLK interaction positively contributes to *lsd1* RCD via $^1O_2$-triggered EX1 signaling suggest a counteractive role of LSD1 toward nuSIB1 and GLKs.

Here, we demonstrate that LSD1, a transcription coregulator and negative regulator of cell death (Dietrich et al., 1994, 1997; Czarnocka et al., 2017), interacts with GLK1/2. LSD1 considerably diminishes the GLK binding activity to promoters of the examined PhANGs in Arabidopsis. In agreement, LSD1-overexpressing plants exhibit significantly

reduced levels of PhANGs, whereas loss of LSD1 causes a notable upregulation of PhANGs relative to WT plants. SA most likely intervenes in the LSD1–GLK interaction through a rapid accumulation of nuSIB1, leading to a nuSIB1–GLKs interaction, enhanced expression of PhANGs, and activation of EX1-dependent $^1O_2$ signaling implicated in cell death. We thus concluded that the stress-associated but mutually exclusive transcription coregulators nuSIB1 (positive regulator) and LSD1 (negative regulator) antagonistically regulate the expression of PhANGs through the physical interaction with GLKs. Such antagonistic regulation of GLK activity by nuSIB1 and LSD1 might be instrumental in sustaining $^1O_2$ homeostasis under SA-associated stress conditions.

Results

LSD1 interacts with the GLK TFs GLK1 and GLK2

The stress hormone SA primes cell death in the *lsd1* mutant in a light-dependent manner, a typical characteristic of most lesion mimic mutants, as manifested by the abrogated cell death by either loss of key SA signaling components (such as NPR1) or overexpression of the bacterial salicylate hydroxylase NahG that metabolizes SA (Muhlenbock et al., 2008; Lv et al., 2019). Upon exposure to various stimuli, including high light, cold, UV-C, red light, hypoxia, and pathogens (Jabs et al., 1996; Dietrich et al., 1997; Muhlenbock et al., 2007, 2008; Huang et al., 2010; Karpinski et al., 2013; Chai et al., 2015; Rusaczonek et al., 2015), *lsd1* mutant plants drastically develop the foliar RCD phenotype. Among those differentially regulated genes prior to the onset of RCD, the SA-induced transcription coregulator nuSIB1 potentiates the expression of PhANGs and stress-related genes by modulating the TF activity of GLK1/2 and WRKY33, respectively (Zarrinpar et al., 2003; Lai et al., 2011; Lv et al., 2019). These data suggest a possible antagonism between LSD1 and nuSIB1 because nuSIB1-driven stress responses occur in the absence of LSD1. In this regard, we sought to test if LSD1 also interacts with GLK1/2 to modulate the expression of PhANGs.

We then generated Arabidopsis WT transgenic plants overexpressing GREEN FLUORESCENT PROTEIN (GFP)-tagged LSD1 under the control of the CaMV 35S promoter (35S) (hereafter *oxLSD1*) to unveil putative LSD1-associated proteins. The immunoblot assay detected the LSD1–GFP fusion protein at the predicted molecular mass of ~46 kDa using an anti-GFP antibody (Supplemental Figure S1). Next, using GFP antibody-conjugated magnetic beads, we co-immunoprecipitated LSD1-GFP and its putative associated proteins from the transgenic plants. The trypsin-digested protein samples were then subjected to tandem mass spectrometry (MS) analyses. The co-immunoprecipitation (Co-IP) coupled to MS analysis using three independent biological replicates identified 217 proteins, which were detected in at least two independent biological replicates, but absent in protein samples of WT and GFP-overexpressing transgenic plants (*35S:GFP*; Supplemental Table S1).

Accordingly, among the 217 proteins, we identified both GLK1 and GLK2 (Supplemental Table S1). In Arabidopsis, GLK1 and its homolog GLK2 share around 50% amino acid sequence identity. Both contain two conserved domains, a DNA-binding domain (DBD) and a GLK1/2-specific C-terminal GCT-box (Supplemental Figure S2; Rossini et al., 2001; Fitter et al., 2002). A domain comparison between GLK1 and GLK2 shows a 90% and 79% identity, respectively (Bravo-Garcia et al., 2009). Therefore, it is not surprising that both GLK1 and GLK2 were detected as putative LSD1-associated proteins. Next, we performed a bimolecular fluorescence complementation (BiFC) assay in *Nicotiana benthamiana* leaves. Since earlier reports showed that LSD1 forms a homodimer (Chai et al., 2015; Czarnocka et al., 2017), we first sought to test the LSD1–LSD1 interaction prior to examining LSD1–GLK interaction. As a result, we confirmed their interaction, as evident in the overlapped signals detected from YELLOW FLUORESCENT PROTEIN (YFP) and blue-fluorescent DNA stain 4′, 6-diamidino-2-phenylindole (DAPI)-stained nucleus, as well as in the cytosol (Figure 1A). Similarly, we observed a YFP signal in *N. benthamiana* leaf coexpressing LSD1- N-terminal part of the YFP (YFP^N) and GLK1 (or GLK2)-C-terminal part of YFP (YFP^C) but exclusively from the nuclei (Figure 1A). We then transiently coexpressed the LSD1-GFP and Myc-tagged GLK1 (GLK1-Myc; or GLK2) in *N. benthamiana* leaves. The resulting Co-IP and immunoblotting analyses further corroborated the LSD1–GLK interaction (Figure 1B). We also purified full-length recombinant proteins of LSD1, GLK1, and GLK2 expressed in *Escherichia coli*. The purified proteins were subjected to gel filtration chromatography (see "Materials and Methods" for details) to confirm the LSD1–GLK interaction in vitro. Gel filtration chromatography assay ensures the separation of proteins according to the difference in size; for instance, a large protein complex shows a faster migration speed with a shorter retention time (or elution volume) than a free protein avoiding complex formation. Indeed, the detected protein peaks (monitored by the UV absorbance at A280) of LSD1–GLK1 protein mix (9–12 mL; Figure 1C) and LSD1–GLK2 protein mix (9–15 mL; Figure 1D) were substantially shifted to the shorter retention time (or elution volume) relative to the protein peaks of LSD1 (15–18 mL), GLK1 (13–16 mL), and GLK2 (13–16 mL) alone. The subsequent sodium dodecyl sulfate-polyacrylamide gel electrophoresis (SDS–PAGE) separation with protein samples eluted from each fraction validated the LSD1–GLK interaction (Figure 1E).

LSD1 interacts with GLK1 and GLK2 through the proline-rich domain

We then generated truncated GLK variants to determine which domain is required for the interaction with LSD1. Prior to the interaction analysis, GLK1/2 and their variants lacking either DBD, potential proline-rich domain (PRD; located between DBD and GCT-box; see "Discussion"), or GCT-box were C-terminally fused with GFP to monitor

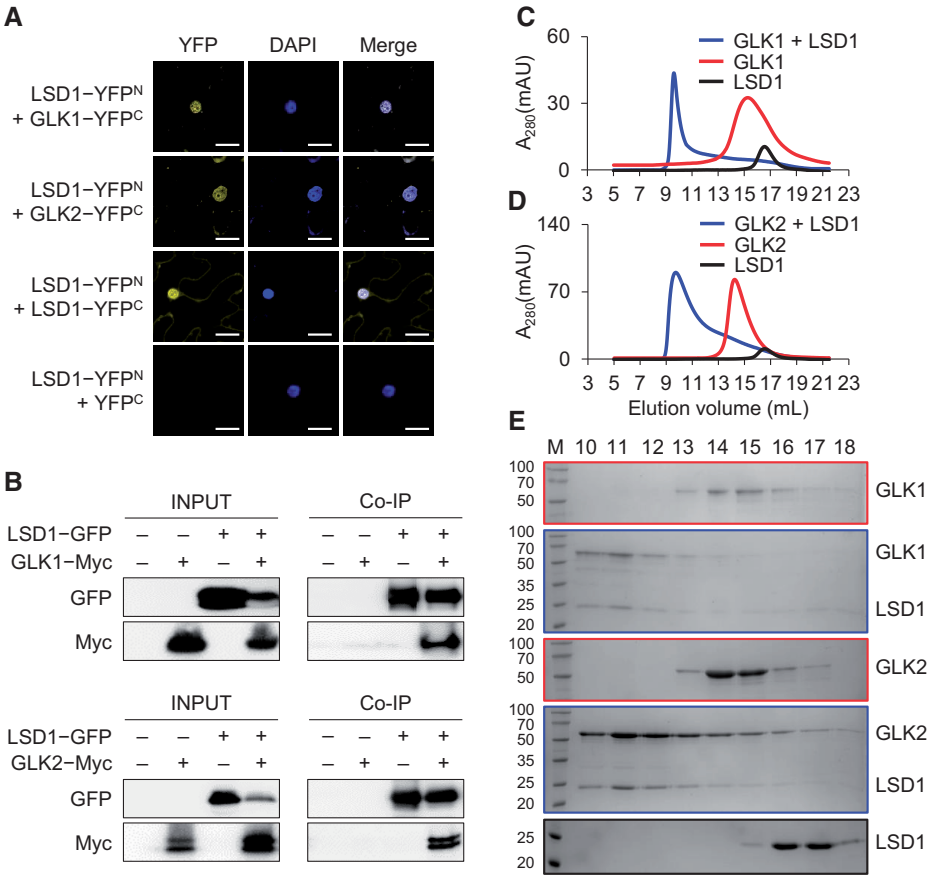

Figure 1 LSD1 interacts with GLK1 and GLK2. A, BiFC assays. The GLK1 or GLK2 fused with the YFP^C were coexpressed with the YFP^N fused with LSD1 in *N. benthamiana* leaves. The combinations of LSD1-YFP^N + LSD1-YFP^C, and LSD1-YFP^N + YFP^C were used as a positive and negative control, respectively. DAPI was used to stain the nucleus. All images were taken at the same scale (scale bars: 25 μm). B, Co-IP analyses using *N. benthamiana* leaves transiently coexpressing LSD1-GFP and GLK1-Myc (or GLK2-Myc). Co-IP was performed using GFP-Trap beads, and the interaction was evaluated by using Myc antibody. C–E, Gel filtration assays showing in vitro interaction between LSD1 and GLK proteins expressed in *E. coli*. Gel filtration profiles of LSD1, GLK1, and LSD1–GLK1 complex (C) and of LSD1, GLK2, and LSD1–GLK2 complex (D). A_{280}(mAU), micro-ultraviolet absorbance at the wavelength of 280 nm. Coomassie blue staining of the peak fractions following SDS–PAGE (E). Numbers on top of SDS–PAGE panels indicate elution volume (mL). M, molecular weight ladder (kDa).

their nuclear localization (Figure 2A; Supplemental Figure S2). Following transient expression, all intact and variants of Arabidopsis GLK1/2 localized in the nucleus in *N. benthamiana* leaves but with a weak cytosolic GFP signal of GCT-box-deleted GLK1 ($GLK1_{\Delta GCT}$) and GLK2 ($GLK2_{\Delta GCT}$) (Supplemental Figure S3). To examine their interaction with Arabidopsis LSD1 protein, various combinations of BiFC constructs, as shown in Figure 2A, were expressed in *N. benthamiana* leaves to observe their interactions under the confocal microscope. The result clearly showed that the PRD of GLK1/2 is indispensable for the interaction with LSD1 (Figure 2B), further verified by Co-IP analyses (Figure 2C). We then generated GLK1/2 variants by C-terminal serial deletions to ascertain the significance of PRD for the interaction (Supplemental Figure S4A). The C-terminal deleted proteins, $GLK1_{\Delta CT}$ and $GLK2_{\Delta CT}$, fused with GFP were localized to the nucleus in *N. benthamiana* leaves (Supplemental Figure S4B). The resulting BiFC and Co-IP analyses confirmed the critical role of PRD for LSD1 interaction, as evidenced by the lack of YFP signal when coexpressing LSD1 and GLK1/2 variants lacking the PRD-including C-terminal part (Supplemental Figure S4, C and D).

Loss of *LSD1* upregulates GLK target genes

Given that GLKs promote the expression of PhANGs (Waters et al., 2009), it is plausible that loss of LSD1 may primarily affect their abundance. To identify affected genes either by loss of LSD1 or of GLK1/2, we compared the differentially expressed genes (DEGs) in *lsd1* and *glk1 glk2* relative to corresponding WT plants using the previously published RNA-seq data (Ni et al., 2017; Lv et al., 2019). The cross-comparison of those DEGs found that a total of 91 genes (Figure 3A; Supplemental Table S2) were shared between the upregulated genes (395, at least twofold) in *lsd1* (Supplemental Table S3) and the downregulated genes (936, at least twofold) in *glk1 glk2* (Supplemental Table S4). The gene ontology (GO) enrichment analysis with the 91 genes for the biological process (BP) revealed that 27 genes were annotated to nine GO terms of which "response to oxygen-containing compound" (*P*-value = 3.31E-08), "photosynthesis

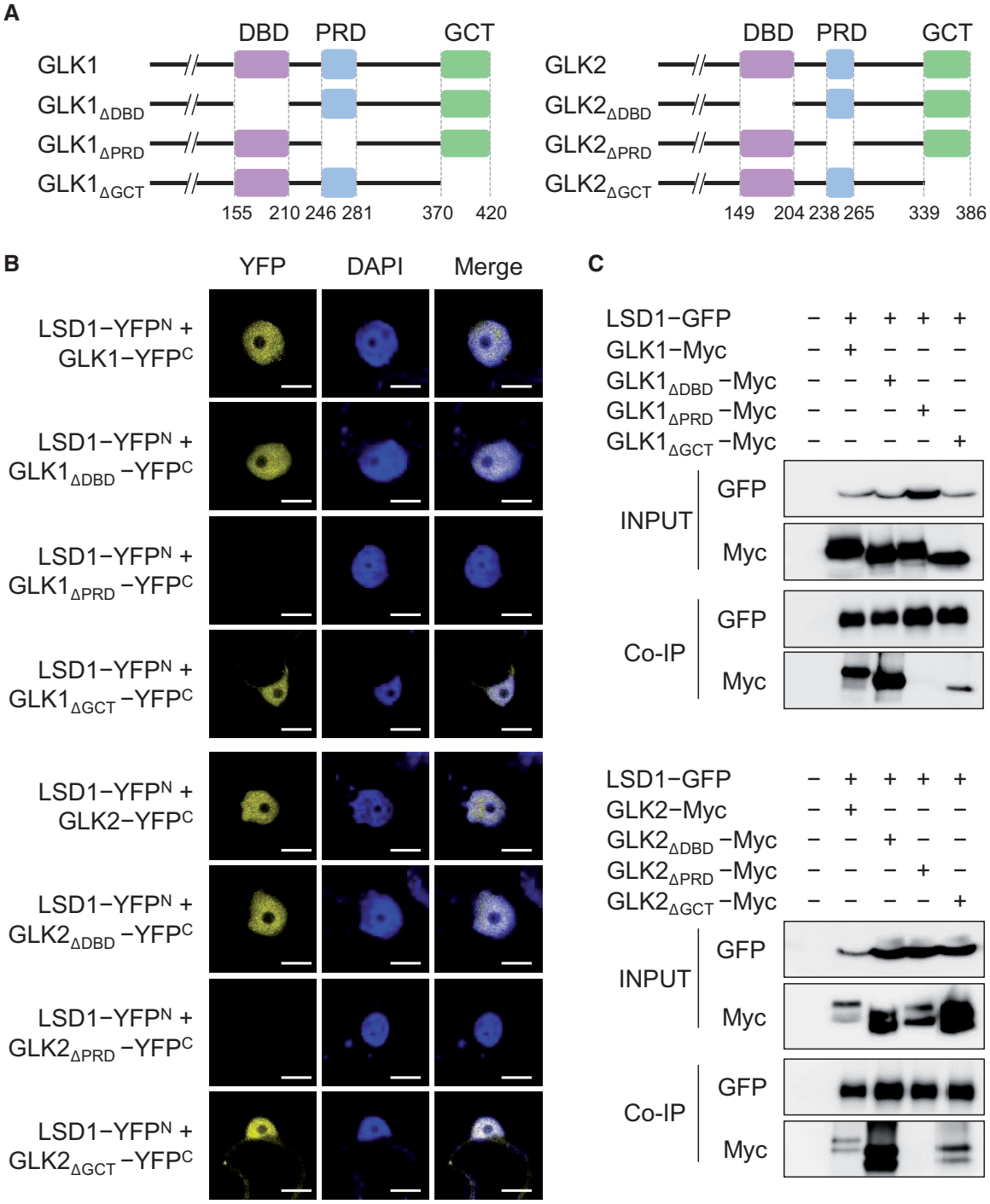

Figure 2 PRD is indispensable for the interaction with LSD1. A, Schematic diagrams show intact GLK1/2 as well as their domain-deleted variants. B, BiFC assays. Each of intact and domain-deleted GLK variants fused with YFP^C was coexpressed with LSD1 fused with YFP^N in *N. benthamiana* leaves. DAPI was used to stain the nucleus. All images were taken at the same scale (scale bars: 10 μm). C, Co-IP analyses using *N. benthamiana* leaves transiently coexpressing LSD1-GFP with the indicated domain-deleted variant of GLK1/2 fused with Myc-tag. GCT-box, GLK/C-terminal box.

and light-harvesting in PSII" (*P*-value = 1.41E-07)," "positive regulation of ROS biosynthetic process" (*P*-value = 4.44E-04), and "Protein-chromophore linkage" (*P*-value = 6.05E-04) were mostly over-represented (Supplemental Figure S5; Supplemental Table S5). Among those genes, we found 7 PhANGs, such as *light-harvesting chlorophyll a/b-binding protein* (*LHCB*) *1.1*, *LHCB2.1*, *LHCB2.2*, *LHCB2.4*, *LHCB3*, *Pchlide oxidoreductase A* (*PORA*), and *magnesium chelatase H subunit* (*GUN5*/*CHLH*). The potentiated expression of PhANGs in *lsd1* versus WT plants is indicative of a negative role of LSD1 in GLK activity. To this end, we also examined the transcript abundance of PhANGs in WT, *glk1 glk2*, and

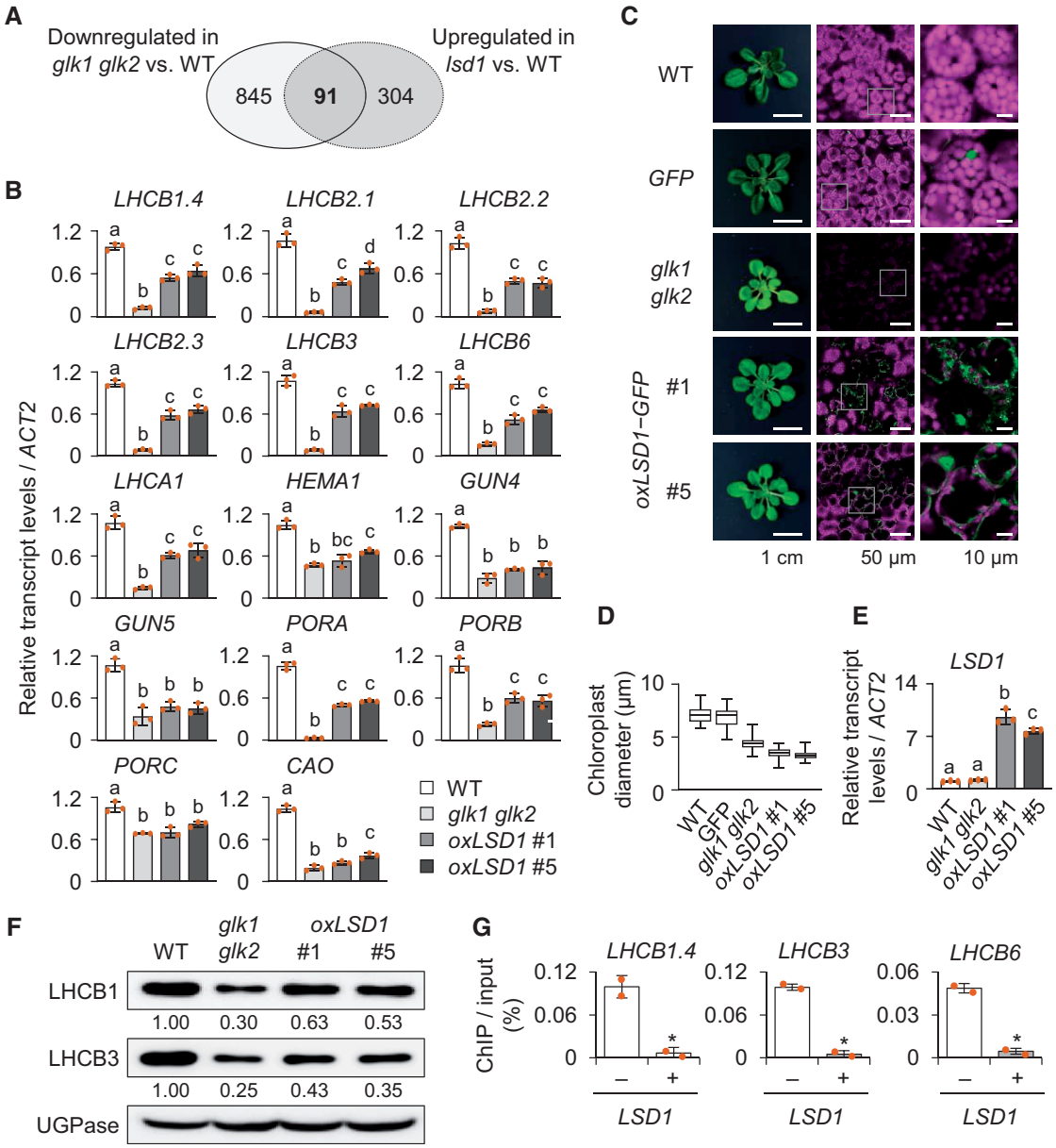

Figure 3 Overexpression of LSD1 negatively affects the expression of GLK target genes and chloroplast biogenesis. A, Venn diagram showing the numbers of uncommon and overlapped genes between upregulated genes (395) in 17-d-old *lsd1* (Lv et al., 2019) and downregulated genes (936) in *glk1 glk2* (Ni et al., 2017). A web-based tool (http://bioinformatics.psb.ugent.be/webtools/Venn/) was used to generate the Venn diagram. B, Relative transcript levels of GLK1 and GLK2 target genes, such as *LHCBs*, *LHCA1*, and chlorophyll synthesis genes including *HEMA1*/*Glu-TR*, *GUN4*, *CHLH*/*GUN5*, *PORA*, *PORB*, *PORC*, and *CAO* were examined in CL-grown 24-d-old WT, *glk1 glk2*, and *oxLSD1* (#1 and #5) plants using RT-qPCR. C, Plant phenotypes (left) and GFP fluorescence (green) of LSD1–GFP fusion proteins merged with chlorophyll autofluorescence signals (red; middle and right) in 24-d-old WT, *glk1 glk2*, and transgenic WT plants overexpressing GFP alone or LSD1-GFP (*oxLSD1* #1 and #5) grown under CL conditions. The small white square boxes in the middle panels were enlarged (right). D, Distribution of chloroplast diameter. At least three confocal images taken from three independent leaves were used to measure the chloroplast diameter. For *oxLSD1*, only mesophyll cells with detectable GFP signals were chosen. Data are shown as box plots (n = at least 38). The horizontal line in the box plot represents median. Box ranges represent first quartile and third quartile, and minimum and maximum values are shown by whiskers. E and F, Relative levels of *LSD1* transcript (E) and LHCB proteins (F) in 24-d-old CL-grown plants of WT, *glk1 glk2*, and *oxLSD1* #1 and #5. UGPase was used as a loading control for the immunoblot analysis in F. Numbers at the bottom of each immunoblot result indicate the relative quantities of LHCB1 or LHCB3 proteins against the control signal of UGPase. For the RT-qPCR analyses in (B) and (E), *ACT2* was used as an internal standard. The values represent means ± standard deviation (SD) (n = 3). Lowercase letters indicate statistically significant differences between mean values ($P < 0.05$, one-way ANOVA with post-hoc Tukey's HSD test). G, ChIP-qPCR results showing the effect of LSD1 overexpression on GLK1 binding to the promoter regions of its target genes (*LHCB1.4*, *LHCB3*, and *LHCB6*). GLK1-Myc was transiently expressed with (+ LSD1) or without LSD1-RFP (– LSD1) in Arabidopsis leaf protoplasts isolated from *lsd1 glk1 glk2* triple mutant. The enrichment value was normalized to the input sample, representing means ± SD from two independent ChIP assays. Asterisks denote statistically significant differences by Student's t test ($P < 0.01$) from the value of – LSD1.

two independent *oxLSD1* transgenic lines (Supplemental Figure S6A) using reverse transcription-quantitative PCR (RT-qPCR). The results indicated that the examined GLK target genes, such as genes encoding light-harvesting chlorophyll *a*/*b* binding proteins (LHCBs in PSII and LHCA1 in PSI) and chlorophyll synthesis enzymes were substantially repressed in *oxLSD1* relative to WT plants (Figure 3B). *oxLSD1* plants exhibited comparable levels of *GLK1* and *GLK2* transcripts relative to WT (Supplemental Figure S6B), implying that the repression of PhANGs likely resulted from the post-translational regulation of GLK1/2. Remarkably, the overexpression of LSD1–GFP fusion proteins in WT prematurely terminated chloroplast development, which is reminiscent of the phenotype observed in *glk1 glk2* double mutant (Figure 3, C and D). Some mesophyll cells with nearly undetectable LSD1-GFP signals showed WT-like chloroplasts (Figure 3C). One explanation might be an ectopic cosuppression of the transgene, which also dilutes the molecular phenotypes (e.g. the transcript levels of PhANGs) in the examined leaf tissue. Two independent *oxLSD1* lines with higher *LSD1* transgene expression than the endogenous *LSD1* in WT plants (Figure 3E) exhibited similar phenotypes, such as partial cosuppression of the transgene, defect in chloroplast biogenesis, and reduced levels of LHCB proteins (Figure 3, C, D, and F).

LSD1 inhibits the DNA-binding activity of GLK1

Regarding that nuclear-localized LSD1 acts as a transcription coregulator and that LSD1 interacts with GLKs, it is conceivable that LSD1 might directly regulate the DNA-binding activity of GLK1/2. Therefore, we conducted a chromatin immunoprecipitation (ChIP) coupled with a qPCR analysis. The relative activity of GLK1 toward its target promoters was examined in the presence or absence of LSD1 using protoplasts isolated from the rosette leaves of *lsd1 glk1 glk2* triple mutant plants. Since GLK1 and GLK2 are highly unstable (Waters et al., 2008; Tokumaru et al., 2017), we used a protoplast transient expression system to ensure sufficient protein expression to elucidate the impact of LSD1 on GLK1 function. The *35S:GLK1-Myc* was transiently coexpressed with either *35S:RED FLUORESCENT PROTEIN* (*RFP*) or *35S:LSD1-RFP* in the protoplasts. ChIP assays were then performed with nuclear lysis from transfected protoplasts. With anti-Myc antibody-conjugated agarose beads, the Myc-tagged protein–DNA complex was pulled down. The immunoprecipitated DNA was then analyzed using qPCR to compare the DNA-binding activity of GLK1 in the presence or absence of LSD1. Afterward, we examined the relative expression levels of well-established GLK target genes such as *LHCB1.4*, *LHCB3*, and *LHCB6* (Waters et al., 2009). The results demonstrated that the presence of LSD1 markedly diminished the DNA-binding activity of GLK1 to promoters of these *LHCB* genes (Figure 3G).

Loss of LSD1 potentiates $^1O_2$-triggered EX1-dependent RS

We next validated the above ChIP assay result in planta. Considering the positive regulation of chlorophyll synthesis by GLK1 (Waters et al., 2009) and the repression of GLK activity by LSD1 (Figure 3), it is tempting to hypothesize that loss of LSD1 might increase the rate of chlorophyll biosynthesis. By revisiting the previously published RNA-seq data (Lv et al., 2019), we noticed that a set of chlorophyll synthesis genes including *glutamyl tRNA reductase* (*HEMA1*/*Glu-TR*), *genome uncoupled 4* (*GUN4*), *GUN5*/*CHLH*, *magnesium protoporphyrin IX monomethyl ester cyclase* (*CHL27*/*CRD1*), *PORA*, and *chlorophyllide a oxygenase* (*CAO*) were markedly upregulated in *lsd1* before the onset of RCD (Figure 4, A and B). We then analyzed the 5-aminolevulinic acid (5-ALA, the common precursor of all tetrapyrroles) synthesis rate in light-grown *lsd1* mutant plants treated with levulinic acid (LA; Nandi and Shemin, 1968), a competitive chemical inhibitor of 5-ALA dehydratase that catalyzes the synthesis of porphobilinogen through the asymmetric condensation of two 5-ALA molecules (Figure 4A). It is important to note that the 5-ALA synthesis is the rate-limiting step for chlorophyll synthesis (Beale and Castelfranco, 1974; Hou et al., 2019; Figure 4A). In view of the fact that FLU protein directly represses Glu-TR activity to inhibit Pchlide accumulation in the dark (Goslings et al., 2004; Figure 4A) and that *flu* mutant plants exhibit a higher 5-ALA synthesis rate in the presence of LA under CL conditions (Goslings et al., 2004), we used *flu* as a positive control.

The 5-ALA synthesis rate was almost comparable in *lsd1* and *flu* seedlings in the presence of LA (Figure 4C). Although it is yet unclear whether the transcriptional upregulation of *HEMA1* is responsible for the 5-ALA accumulation in *lsd1*, the concurrent loss of both *FLU* and *LSD1* further increased the 5-ALA synthesis rate under CL conditions (Figure 4C). Since Pchlide levels in the dark would indirectly reflect chlorophyll biosynthesis rate owing to the absence of the enzyme(s) involved in Pchlide turnover (Forreiter and Apel, 1993), we measured Pchlide levels in dark-incubated plants of WT, *flu*, *lsd1*, and *lsd1 flu* using a high-performance liquid chromatography analysis. As anticipated, Pchlide was highly upregulated in the *flu* mutant background, as demonstrated earlier (Meskauskiene et al., 2001; Figure 4D). The loss of LSD1 raises the Pchlide level (approximately a 1.5-fold increase) in both WT and *flu* mutant backgrounds. The presence of FLU protein in *lsd1* seems to prevent the drastic accumulation of Pchlide in the dark. Collectively, these results corroborate the negative role of LSD1 toward GLK activity, which seems to be, at least in part, required for tetrapyrrole homeostasis.

We then hypothesized that the SA-induced nuSIB1-GLK-driven upregulation of PhANGs and the higher chlorophyll synthesis rate by *FLU* mutation might further enhance $^1O_2$ levels in chloroplasts in *lsd1 flu* plants grown under CL

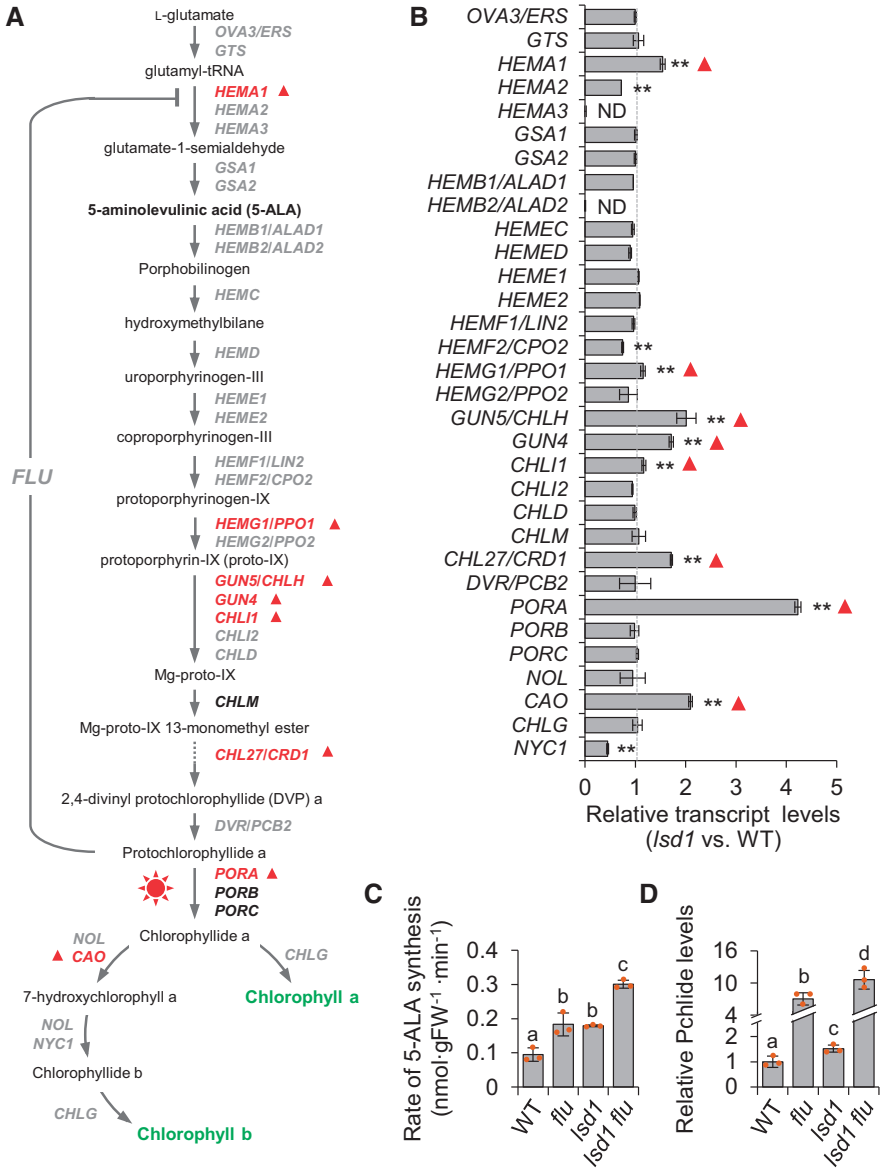

Figure 4 *LSD1* mutation leads to the transcriptional upregulation of chlorophyll synthesis genes. A, A schematic representation of the chlorophyll synthesis pathway. B, The expression levels of chlorophyll synthesis genes represented in (A) were obtained from our previous study (Lv et al., 2019), and the relative transcript levels of chlorophyll synthesis genes in 17-d-old CL-grown *lsd1* mutants compared to WT are represented. Error bars indicate SD (n = 3). Asterisks indicate statistically significant differences (*$P < 0.05$; **$P < 0.01$) in the *lsd1* mutant determined by Student's t test relative to WT. ND: nondetected. Red triangles in (A) and (B) indicate the significantly upregulated genes in the *lsd1* mutant compared to WT. C, Levels of 5-ALA synthesis rate under CL conditions. The 5-ALA synthesis rate was measured in 16-d-old plants of WT, *flu*, *lsd1*, and *lsd1 flu*. D, Relative levels of Pchlide in 10-d-old plants of WT, *flu*, *lsd1*, and *lsd1 flu* grown under CL and then transferred to the dark for 8 h. Values in (C) and (D) represent means ± SD (n = 3). Lowercase letters indicate significant differences between the indicated genotypes ($P < 0.05$, one-way ANOVA with post-hoc Tukey's HSD test).

conditions before the onset of RCD. Indeed, compared to *lsd1* plants, *lsd1 flu* double mutant plants exhibited accelerated RCD (Figure 5A), which was radically reduced in *lsd1 flu ex1* compared to *lsd1 flu* plants, indicating $^1O_2$ was the prime cause of the reinforced RCD in *lsd1 flu*. This result coincided with the intensity of maximum fluorescence (Fm) of PSII (Figure 5A), PSII maximum efficiency (Fv/Fm) (Figure 5B), and the abundance of $^1O_2$-responsive genes (SORGs; Dogra et al., 2017; Figure 5C).

SA-induced SIB1 interrupts LSD1–GLK1 interaction

Since SIB1-mediated genomes uncoupled expression of PhANGs and PhAPGs largely contributes to *lsd1* RCD via $^1O_2$ signaling (Lv et al., 2019), we hypothesized that nuSIB1 would counteractively modulate LSD1–GLK interaction to reinforce the expression of PhANGs. Considering its rapid turnover via UPS (Li et al., 2020), nuSIB1 may promptly intervene in this LSD1–GLK interaction, resulting in nuSIB1–GLK interaction and reinforced expression of PhANGs,

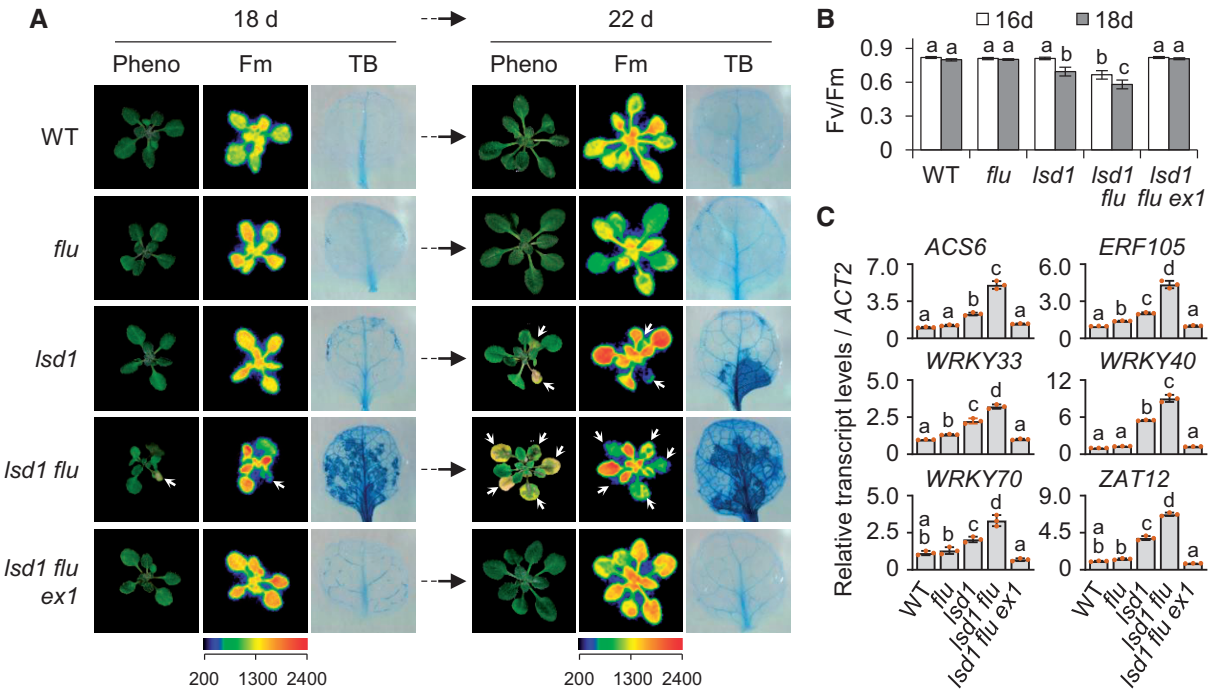

Figure 5 Loss of LSD1 potentiates $^1O_2$-triggered EX1-dependent RS. A, WT, *flu*, *lsd1*, *lsd1 flu*, and *lsd1 flu ex1* plants were grown on MS medium under CL conditions (100 μmol·m^{-2}·s^{-1}). The RCD phenotype (Pheno, left) and the chlorophyll F_m of PSII (middle) were monitored in the whole plants at the indicated time points. The dead cells in the first or second leaves from the genotypes were visualized via TB staining (right). Images are representative phenotypes. B, The first or second leaves from each genotype were harvested at the indicated time points to measure the maximum photochemical efficiency of PSII (F_v/F_m). Data represent means ± SD (n = 10). C, Expression levels of selected SORGs were examined by RT-qPCR in 18-d-old plants. *ACT2* was used as an internal standard. Data represent means ± SD (n = 3). Lowercase letters in (B) and (C) indicate statistically significant differences between mean values ($P < 0.05$, one-way ANOVA with post-hoc Tukey's HSD test).

thereby contributing to cell death (Lv et al., 2019). Alternatively, SA may interfere with LSD1–GLK interaction, for instance, through alteration of protein conformation of LSD1 or GLKs or both. In fact, a previous report showed a redox-sensitive reconfiguration of LSD1 and concurrent change of its interactome (Czarnocka et al., 2017). Thus, we examined how SA impacts the LSD1–GLK1 interaction in Arabidopsis leaf protoplasts isolated from WT and *sib1* mutant plants. The result that SA substantially hindered the LSD1–GLK1 interaction in WT but not in *sib1* (Figure 6A) suggested that nuSIB1 rather than SA interrupts LSD1–GLK1 interaction. To further elucidate an antagonistic action of nuSIB1 toward LSD1–GLK1 interaction, a dose-dependent impact of nuSIB1 was examined. For this, LSD1-GFP and GLK1-Myc were transiently coexpressed in Arabidopsis leaf protoplasts, along with different amounts of free RFP or SIB1-RFP. It should be noted that increasing doses of RFP or SIB1-RFP reduce the expression of LSD1-GFP and GLK1-Myc, probably as a consequence of diminished transfection efficiency due to the presence of the additional constructs (Figure 6B). Nonetheless, the relative amount of GLK1-Myc protein co-immunoprecipitated with LSD1-GFP was quantified using ImageJ following immunoblot analysis (Figure 6C). The results showed a SIB1 dose-dependent inhibition of the LSD1–GLK1 interaction.

One possible scenario for the nuSIB1-dependent interruption of LSD1–GLK interaction is that SA-induced nuSIB1 may directly interact with LSD1, releasing GLK1 and GLK2 in the nucleus. The free GLK1/2 may interact with excess nuSIB1, promoting the expression of PhANGs. However, while the LSD1–LSD1 interaction was apparent, no interaction between LSD1 and nuSIB1 was observed (Supplemental Figure S7). Then we assumed that SA-induced nuSIB1 might compete with LSD1 to bind to the PRD of GLK1 and GLK2. We then carried out Co-IP analyses to investigate if PRD is required for the interaction with SIB1. The result showed that the N-terminal region excluding all three domains is sufficient to interact with nuSIB1 (Supplemental Figure S8, A and B). Since the N-terminal part contains a nuclear localization signal (Zhang et al., 2021a), we ended further defining the minimum length of the N-terminal necessary for the interaction with nuSIB1. It is likely that SA-induced nuSIB1 competitively interacts with GLK1 and GLK2 through the N-terminal part, which consequently enhances the expression of PhANGs and the $^1O_2$ level, thereby activating an EX1-mediated cell death response (Figure 7). The rapid turnover of nuSIB1 via UPS (Li et al., 2020) might result in LSD1–GLK interaction and restore the expression levels of PhANGs.

Discussion

Besides their essential role in chloroplast biogenesis and photosynthesis, multiple lines of evidence demonstrate that GLKs function in plant stress responses (Nagatoshi et al.,

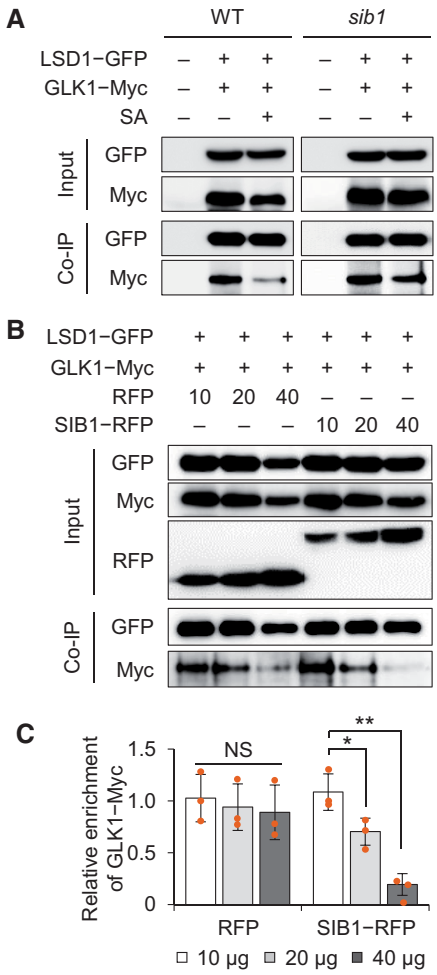

Figure 6 SA-induced SIB1 intervenes in LSD1–GLK interaction. A, The effect of the SA-induced nuSIB1 on the LSD1–GLK1 interaction. For Co-IP analyses, *35S:LSD1-GFP* and *35S:GLK1-Myc* were transiently coexpressed in Arabidopsis leaf protoplasts. The protoplasts were treated with either mock or 0.2 mM SA (for 5 h). B, The dose-dependent impact of SIB1 on the LSD1–GLK1 interaction. As indicated, *35S:LSD1-GFP* and *35S:GLK1-Myc* were coexpressed in Arabidopsis leaf protoplasts isolated from WT plants together with different amounts (10, 20, or 40 μg, respectively) of a plasmid containing either free *35S:RFP* or *35S:SIB1-RFP*. The subsequent Co-IP and immunoblot results are shown. Three independent experiments were conducted with similar results, and representative results are shown in (A) and (B). C, The signal intensity of eluted GLK1-Myc (from triplicate immunoblots in (B)) versus its input signal was quantified using the ImageJ software. Data are means ± SD ($n = 3$). Asterisks denote statistically significant differences by Student's *t* test (*$P < 0.05$, **$P < 0.01$, NS, not significant).

2016; Liu et al., 2018; Ahmad et al., 2019; Lee et al., 2021; Zhang et al., 2021b), evoking an intriguing proposal that GLK may serve as a master switch in synchronously regulating photosynthesis and stress responses. Moreover, recent studies discovered an unexpected function of GLKs toward plant immune responses. The steady-state levels of SA-responsive genes are significantly lower in GLK1-overexpressing (*oxGLK1*) Arabidopsis transgenic plants relative to WT plants (Savitch et al., 2007). Hence, the *oxGLK1* plants are susceptible to the biotrophic pathogen *Hyaloperonospora arabidopsidis* Noco2, while *glk1 glk2* double knockout mutant plants are more resistant compared to WT plants (Murmu et al., 2014). However, other studies reported that GLKs confer resistance toward the cereal fungal pathogen *Fusarium graminearum* (Savitch et al., 2007), necrotrophic fungal pathogen *Botrytis cinerea* (Murmu et al., 2014), and the Cucumber mosaic virus (Han et al., 2016). These findings indicate that multiple regulatory circuits (positive and negative) may differently modulate GLK activity toward various microbial pathogens.

We previously reported that the positive regulator of SA signaling and transcription coregulator nuSIB1 interacts with GLKs and WRKY33 to reinforce the expression of PhANGs and SA-responsive genes, respectively, upon an increase in cellular SA level (Lv et al., 2019; Li et al., 2020). In contrast, cpSIB1 interacts with SIGMA FACTOR 1 (SIG1) polymerase to repress the expression of PhAPGs (Morikawa et al., 2002; Xie et al., 2010; Lv et al., 2019). The genomes-uncoupled expression of PhANGs and PhAPGs heightens the PSII photoinhibition, thereby escalating the highly reactive oxygen species, specifically $^1O_2$. $^1O_2$ then contributes to SA-driven plant stress responses via EX1-mediated RS, which is shown to reinforce RCD phenotype in *lsd1* mutant (Dogra et al., 2019; Lv et al., 2019). Since the SA receptor NPR1 is required to induce the expression of *SIB1* (Xie et al., 2010), EX1-mediated $^1O_2$ signaling is likely to be one of the downstream events led by SA and NPR1.

We now showed that LSD1 interacts with GLK1 and GLK2 TFs in the nucleus (Figure 1A). Besides their transcriptional regulation (e.g. by GUN1-mediated RS), multiple proteins posttranslationally modulate GLK activity (Tang et al., 2016; Tokumaru et al., 2017; Zhang et al., 2021a). The C-terminal GCT-box drives GLK homo- or hetero-dimerization in maize (*Zea mays* L.; Rossini et al., 2001). The *turnip yellow mosaic virus* protein P69 binds to the GLK1/2 GCT-box, repressing PhANGs and chloroplast biogenesis in Arabidopsis (Ni et al., 2017). On the contrary, BRASSINOSTEROID INSENSITIVE 2-dependent GLK phosphorylation promotes chloroplast biogenesis by stabilizing GLK proteins in Arabidopsis (Zhang et al., 2021a). These reports indicate that both DBD and GCT-box in GLK1/2 are involved in protein–protein interaction. Notably, the inter-domain region of GLK1 and GLK2 are proline-enriched (Figure 2A; Supplemental Figure S2). Since proline residues provide protein-docking sites (Siligardi and Drake, 1995; Zarrinpar et al., 2003), we anticipated the PRD as an additional candidate domain required for the interaction with LSD1. The ensuing BiFC and Co-IP assays verified that the PRD is central for interacting with LSD1. GLK1 and GLK2 lacking DBD and GCT-box but retaining PRD interacted with LSD1, but complete loss of PRD abolished these interactions (Figure 2, B and C). Besides, the association of GLK2 with the CUL4-DDB1-based E3 ligase complex promotes UPS-mediated GLK2 turnover in tomato (*Solanum lycopersicum* L.; Tang et al., 2016). The COP1 and UPS-mediated GLK1 degradation was also reported in Arabidopsis plants

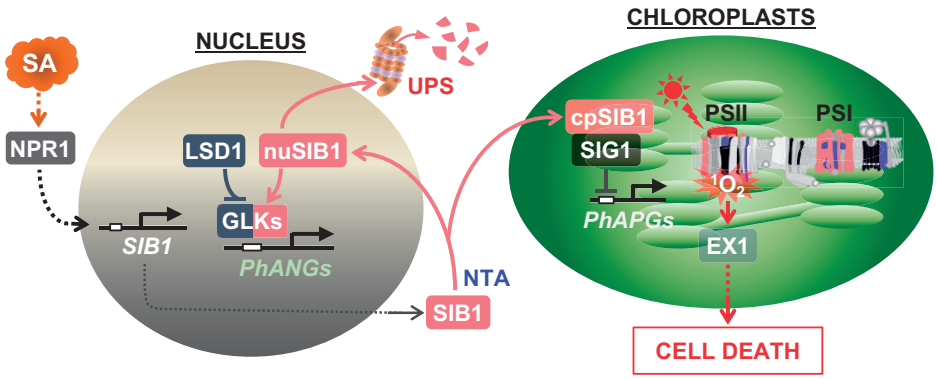

Figure 7 Proposed model elucidating the counteractive regulation of GLKs by LSD1 and nuSIB1. LSD1–GLK interaction is required for negative regulation of GLK activity to fine-tune the expression of PhANGs, including LHCBs and chlorophyll synthesis genes. Under SA-increasing stress conditions, the NPR1-induced and NTA-stabilized nuSIB1 intervenes in LSD1–GLK interaction to reinforce the expression of PhANGs, while the cpSIB1 represses the expression of PhAPGs by interacting with SIG1 (Morikawa et al., 2002; Lv et al., 2019; Li et al., 2020). The resulting uncoupled expression of PhANGs and PhAPGs aggravates PSII photoinhibition and increases $^1O_2$ level in chloroplasts, enabling EX1-mediated RS to activate the expression of SORGs and cell death response (Kim et al., 2012; Lv et al., 2019). While NTA renders nuSIB1 more stable, UPS promotes the proteolysis of nuSIB1 (Li et al., 2020), restoring LSD1–GLK interaction to avoid an excess of PhANG expression and $^1O_2$ accumulation. The counteractive regulation of GLKs by nuSIB1 and LSD1, along with posttranslational regulation of nuSIB1 stability, seems vital to modulate $^1O_2$ levels in chloroplasts during and after SA-increasing stress conditions.

with long-term abscisic acid (ABA) treatment (Lee et al., 2021). Interestingly, one latest work showed that WRKY75 directly represses *GLK* expression during leaf senescence (Zhang et al., 2021b). The ABA-induced SIB1 and its homolog SIB2 interact with and inhibit WRKY75 activity, enabling the expression of GLKs in response to ABA. The antagonistic regulation of GLKs expression by SIB1/2 and WRKY75 was proposed to be essential in controlling ABA-mediated leaf senescence and seed germination. These findings by other groups and our data suggest that the GLKs are common targets of development or stress signaling to modulate chloroplast homeostasis. As emerging notion strongly supports the role of chloroplasts as environmental sensors, such modulation of GLK activity and stability would also significantly affect chloroplast-mediated plant stress responses.

Loss of LSD1 potentiated the expression of GLK target genes such as PhANGs (Figures 3, A and 4, A and B) and increased the 5-ALA synthesis rate compared to WT plants (Figure 4C). Conversely, LSD1 overexpression repressed the expression of PhANGs (Figure 3B). These results were consistent with *oxLSD1* plant phenotypes exhibiting prematurely terminated chloroplast development and reduced LHCB levels (Figure 3, C–F). Moreover, LSD1 overexpression repressed GLK1 binding activity to its target promoters (Figure 3G). Therefore, the effects of loss- and gain-of-function of LSD1 toward the expression of GLK target genes also suggest a steady-state LSD1–GLK interaction in WT plants grown under normal growth conditions. Given that the elevated expression of PhANGs directed by nuSIB1–GLK interaction contributes to *lsd1* RCD (Lv et al., 2019), it was tempting to hypothesize that SA-induced nuSIB1 interferes with LSD1–GLK interaction. Indeed, the Co-IP assay confirmed the negative impact of nuSIB1 accumulation on LSD1–GLK interaction (Figure 6). It has been shown that the PRD domain provides the sequence-specific docking site for interacting proteins without the requirement of a high-affinity interaction (Saraste and Musacchio, 1994; Siligardi and Drake, 1995; Zarrinpar et al., 2003). The sequence-specific but low-affinity interaction at the proline-rich region might allow a highly reversible interaction between LSD1 and GLKs, enabling SA-induced nuSIB1 to rapidly intervene in this interaction through the N-terminus of GLKs (Figure 2; Supplemental Figures S4 and S8). Such versatile regulation of nuSIB1 stability and an antagonistic mode of action of nuSIB1 and LSD1 toward GLK1/2 might be vital to maintain $^1O_2$ homeostasis in chloroplasts and to induce SA-driven stress responses under fluctuating environmental conditions (Figure 7).

Our findings also raise a plausible idea that GUN1-mediated RS would largely contribute to plant stress responses because the signaling primarily represses the expression of *GLK1* and *GLK2* once the foliar plastid function is interrupted (see "Introduction"). Consistent with this notion, *gun1* mutant plants exhibit an increased susceptibility toward heat, water, drought, cold, and high-light stresses with enhanced cellular ROS levels (Miller et al., 2007; Cheng et al., 2011; Zhang et al., 2011, 2013; Tang et al., 2014). In fact, the phenotype of the *gun1* mutant is quite similar to *lsd1* in terms of the regulation of tetrapyrrole synthesis (Figure 4, C and D; Shimizu et al., 2019), which could perhaps account for its susceptibility to various stress factors. Nonetheless, the multifaceted interactions between GLK1/2 and the antagonistic modules nuSIB1 and LSD1, as well as other stress-related proteins, may be accountable for the altered *gun1* phenotype to various stress factors. The enhanced expression of *GLK1* and *GLK2* may increase the level of $^1O_2$ if nuSIB1 is accumulated and intervene in LSD1–GLK interaction in *gun1*. The $^1O_2$-triggered EX1-mediated RS might then modulate plant stress responses in *gun1* mutant plants under SA-increasing stress conditions. In this regard, study of *gun1* may provide further insight into how

chloroplast RS pathways mediated by GUN1 and EX1 coordinate SA-mediated plant stress responses through GLK1/2 and $^1O_2$, respectively.

Materials and methods

Plant materials and growth conditions

The seeds used in this study were derived from Arabidopsis (*A. thaliana*) Columbia-0 ecotype and were harvested from plants grown under CL (100 μmol·m^{-2}·s^{-1}) at 22 ± 2°C. Arabidopsis mutant seeds used in this study, including *lsd1-2* (SALK_042687; Lv et al., 2019), *glk1 glk2* (*Atglk1.1*; *Atglk2.1*; Fitter et al., 2002), and *ex1* (SALK_002088; Lee et al., 2007) were obtained from the Nottingham Arabidopsis Stock Centre. *flu5c* has been described previously (Meskauskiene et al., 2001). The double and triple mutants in the *lsd1-2* background including *lsd1 flu*, *lsd1 flu ex1*, and *lsd1 glk1 glk2* were generated by crossing the homozygous plants. The genotypes of all mutants were confirmed by PCR-based analyses. Primer sequences used for PCR are listed in Supplemental Table S6.

Seeds were surface sterilized with 70% (v/v) ethanol containing 0.05% (v/v) Triton X-100 (Sigma-Aldrich, St Louis, MO, USA) for 10 min and washed 5 times with sterile distilled water. The sterile seeds were plated on Murashige and Skoog (MS) medium (Duchefa Biochemie, Haarlem, Netherlands) with 0.7% (w/v) agar (Duchefa Biochemie) and stratified at 4°C in darkness for 2 d prior to placing in a growth chamber (CU-41L4; Percival Scientific, Perry, IA, USA) with CL condition.

Generation of *LSD1* overexpression lines

The stop-codon-less *LSD1* coding sequence (CDS) was cloned into the modified pCAMBIA3300 binary vector containing the 35S promoter, an NcoI restriction site, and the *EGFP*. Arabidopsis stable transgenic lines were generated by a floral dip transformation procedure (Clough and Bent, 1998) with *Agrobacterium tumefaciens* strain GV3101. Homozygous transgenic lines were selected on MS medium containing 12.5 mg L^{-1} glufosinate-ammonium (Sigma-Aldrich).

RNA extraction and RT-qPCR

Total RNA was isolated from leaf tissues using the Spectrum Plant Total RNA Kit (Sigma-Aldrich) according to the manufacturer's instructions. The concentration of RNA was determined using the ultraviolet-visible spectrophotometer (NanoDrop, Thermo Fisher Scientific), and the quality of RNA was evaluated by measuring the A260/A280 ratio. cDNA synthesis was performed with 1 μg of total RNA using the PrimeScript RT Reagent Kit (Takara, Shiga, Japan) following the manufacturer's instructions. The RT-qPCR was performed on QuantStudio Flex Real-Time PCR System (Applied Biosystems, Waltham, MA, USA) using iTaq Universal SYBR Green PCR master mix (Bio-Rad, Hercules, CA, USA). The relative transcript level was calculated by the ddCt method (Livak and Schmittgen, 2001) and normalized to the *ACTIN2* (AT3G18780) gene transcript level. The sequences of the primers used for RT-qPCR are listed in Supplemental Table S6.

Co-IP assay

Co-IP assays were performed using *N. benthamiana* or Arabidopsis leaf protoplasts transiently coexpressed with the indicated combination of proteins. For the Co-IP assays in *N. benthamiana*, the *35S:LSD1-sGFP*, *35S:SIB1-sGFP*, *35S:GLK1-4 × Myc*, and *35S:GLK2-4 × Myc* constructs were created as described previously (Lv et al., 2019). Briefly, pDONR221/Zeo entry vector (Thermo Scientific Waltham, MA, USA) containing the stop codon-less full-length CDS of *LSD1*, *SIB1*, *GLK1*, or *GLK2* was recombined into the destination vector pGWB605 for C-terminal fusion with sGFP or into pGWB617 for C-terminal fusion with 4 × Myc through the Gateway LR reaction (Thermo Scientific). For the *35S:GLK1-4 × Myc* (or *sGFP*) and *35S:GLK2-4 × Myc* (or *sGFP*) constructs, a linker DNA encoding Gly–Gly–Ser–Gly–Gly–Ser was added between *4xMyc* (or *sGFP*) tag and GLK1 or GLK2 to increase conformational flexibility of the fusion protein as described previously (Tokumaru et al., 2017). The same procedures were used to create the constructs containing CDSs encoding domain-deleted or C-terminally truncated variants of GLK1 and GLK2. The different combinations of selected vectors were coexpressed in 4-week-old *N. benthamiana* leaves by *Agrobacterium*-mediated leaf infiltration as previously described by Boruc et al. (2010). For the Co-IP assays in Arabidopsis leaf protoplasts, the *35S:LSD1-eGFP*, *35S:GLK1-4 × Myc*, *35S:SIB1-RFP*, and *35S:LSD1-RFP* were cloned into the pSAT6 vector (Tzfira et al., 2005). The isolation and transfection of Arabidopsis leaf protoplasts were performed as described previously (Yoo et al., 2007). The indicated combination of vectors was cotransfected into protoplasts (3 × 10^6) isolated from 4-week-old plants of WT or *sib1*.

Total protein was extracted using an IP buffer containing 50 mM Tris–HCl (pH 7.5), 150 mM NaCl, 0.5-mM EDTA, 10% (v/v) glycerol, 1% (v/v) Nonidet P-40, 1% (w/v) deoxycholate, 0.1% (w/v) SDS, 1 × cOmplete protease inhibitor cocktail (Roche, Basel, Switzerland), 1-mM PMSF, and 50-μM MG132. The protein extracts were incubated with 20 μL of GFP-Trap magnetic agarose beads (GFP-TrapMA, Chromotek, Munich, Germany) for 2 h at 4°C by vertical rotation (10 rpm). After incubation, the beads were washed 5 times with the washing buffer containing 10 mM Tris–HCl (pH 7.5), 150-mM NaCl, 0.5 mM EDTA, 1-mM PMSF, 50-μM MG132, and 1 × cOmplete protease inhibitor cocktail. The immunoprecipitated proteins were then eluted with 2 × SDS protein sample buffer [120 mM Tris–HCl (pH 6.8), 20% (v/v) glycerol, 4% (v/w) SDS, 0.04% (v/w) bromophenol blue, and 10% (v/v) β-mercaptoethanol] for 10 min at 95°C. The eluates were subjected to 10% SDS–PAGE gels, and the interaction between coexpressed proteins was examined by immunoblot analyses using a mouse anti-Myc monoclonal antibody (1:10,000; Cell Signaling Technology, Danvers, MA, USA), a rat anti-RFP monoclonal antibody (1:10,000; Chromotek), and a mouse anti-GFP monoclonal antibody (1:5,000; Roche).

Protein extraction and immunoblot analysis

Total proteins were extracted from 100 mg of foliar tissues with the IP buffer and quantified with a Pierce BCA protein assay kit (Thermo Fisher Scientific). Afterward, 20 μg total protein was separated on 10% SDS–PAGE gels and blotted onto Immun-Blot PVDF membrane (Bio-Rad). LSD1-GFP, LHCB1, and LHCB3 were immunochemically detected with mouse anti-GFP (1:10,000; Roche), rabbit anti-LHCB1 (1:5,000; Agrisera, Vännäs, Sweden), and rabbit anti-LHCB3 (1:5,000; Agrisera) antibodies, respectively. The UDP-glucose pyrophosphorylase (UGPase) detected with rabbit anti-UGPase (1:3,000; Agrisera) was used as a loading control.

Confocal laser-scanning microscopy

The GFP, YFP, chlorophyll, and DAPI fluorescence signals were detected by confocal laser-scanning microscopy analysis using TCS SP8 (Leica Microsystems, Wetzlar, Germany). GFP and YFP were excited using an argon laser at a wavelength of 488 and 514 nm, respectively, and emission of their fluorescence was collected at 500–550 nm for GFP and 520–570 nm for YFP. DAPI was excited by a violet (405 nm) laser line, and its emission was collected at 430–480 nm. Chlorophyll autofluorescence was detected between 650 and 750 nm with a 488 nm laser line for excitation. All the images were obtained and processed with Leica LAS AF Lite software, version 2.6.3 (Leica Microsystems).

BiFC assay

BiFC assays were conducted with a split-YFP system in *N. benthamiana* leaves, as described previously (Lu et al., 2010; Lee et al., 2020). Briefly, the pDONR/Zeo entry vectors (Thermo Fisher Scientific) containing CDSs lacking the termination codon of intact forms, domain-deleted, or C-terminally truncated variants of GLK1 and GLK2 were recombined into the destination vector pGTQL1221 through Gateway LR reaction. The same procedure was done to recombine the pDONR221/Zeo entry vector containing the *LSD1* CDS lacking the terminal codon into the pGTQL1211. For the BiFC assay, *A. tumefaciens* mixtures carrying the appropriate constructs were infiltrated into 4-week-old *N. benthamiana* leaves. The presence of YFP fluorescence signals was evaluated by confocal laser-scanning microscopy analysis.

ChIP-qPCR assays

ChIP assays were performed using Arabidopsis leaf protoplasts as described previously (Yoo et al., 2007; Lee et al., 2017; Lv et al., 2019). Briefly, 1 mg of pSAT6 vectors containing *35S:GLK1-4 × Myc* DNA were transfected with or without pSAT6 vector containing *35S:LSD1-RFP* DNA into Arabidopsis leaf protoplasts (2×10^7) isolated from 4-week-old *lsd1 glk1 glk2* triple mutant plants grown under 10-h light/14-h dark conditions at a light intensity of 100 μmol $m^{-2}s^{-1}$. Afterward, the protoplasts were incubated at 24°C for 16 h under dim light conditions. The protoplast chromatins were crosslinked by 1% (v/v) formaldehyde in 1 × PBS (pH 7.4) for 10 min and quenched with 0.1 M glycine for 5 min. After isolating nuclei from the protoplasts, the chromatins were sheared by sonication into an average size of around 500 bp. The lysates were diluted with 10 × ChIP dilution buffer [1% (v/v) Triton X-100, 2 mM EDTA, 20 mM Tris–HCl (pH 8.0), 150 mM NaCl, 50 μM MG132, 1 mM PMSF, and 1 × protease inhibitor cocktail] and precleared by incubation with 50 μL Protein-A agarose beads/Salmon sperm DNA (Millipore, Burlington, MA, USA) at 4°C for 1 h. The samples were then incubated with anti-Myc monoclonal antibodies (1:10,000; Cell Signaling Technology) at 4°C overnight. To determine the nonspecific binding of DNA on beads, ChIP assays were also performed without antibodies. After washing the beads, the immunocomplexes were eluted with elution buffer containing 1% (w/v) SDS and 100 mM $NaHCO_3$. The eluates were treated with proteinase K for 1 h at 37°C after reverse cross-linking. The bound DNA fragments were purified as previously described by Lee et al. (2017) and precipitated with ethanol in the presence of glycogen. The purified DNA was dissolved in water. qPCR analyses were performed on bound and input DNAs. The primers for each tested gene are listed in Supplemental Table S6. The amount of DNA enriched by the anti-Myc antibody was calculated in comparison with the respective input DNA used for each ChIP analysis. Afterward, the enrichment was calculated by normalizing against the corresponding control sample (without antibody).

Production of recombinant proteins

To produce recombinant proteins of LSD1, GLK1, and GLK2, the CDSs of genes were cloned into the modified pET21b (Novagen, Madison, WI, USA) expression vector after adding a cleavage site for the tobacco etch virus (TEV) protease to the 5′-end of the CDSs. The recombinant proteins with a cleavable N-terminal 10 × His-MsyB tag were expressed in *E. coli* BL21 (DE3). After culturing the cells at 37°C until an OD_{600} of 0.6, recombinant proteins were induced by adding 0.3 mM isopropyl-β-D-thiogalactopyranoside for 12 h at 16°C. Cells were pelleted by centrifugation and resuspended with buffer A [(50 mM Tris (pH 8.0), 200-mM NaCl, and 1-mM PMSF]. The cells were lysed by a high-pressure homogenizer at 600–800 bar and then centrifuged at 17,000 rpm for 50 min. Each soluble fraction was passed over a Ni–NTA column (Novagen) and eluted with buffer containing 25 mM Tris (pH 8.0), 200 mM NaCl, and 200 mM Imidazole. Subsequently, the eluates containing recombinant proteins with 10 × His-MsyB tag were further purified by an anion-exchange column (Source-15Q; GE Healthcare, Chicago, IL, USA). The 10 × His-MsyB tag was cleaved by TEV protease at 4°C overnight and removed by an anion-exchange column. Untagged recombinant proteins were then concentrated and further purified by size-exclusion chromatography (Superdex 200 Increase10/300 GL; GE Healthcare) in buffer containing 20-mM Tris (pH 8.0), 200-mM NaCl, and 3-mM DTT. The peak fractions of each protein were pooled together and used for gel filtration assay.

Gel filtration assay

The recombinant proteins purified as described above were subjected to gel filtration assay (Superdex 200 Increase10/300 GL; GE Healthcare) in buffer containing 20-mM Tris (pH 8.0), 200-mM NaCl, and 3-mM DTT. A mixture of the purified LSD1 and GLK1 (or GLK2) proteins was incubated at 4°C for 1 h before gel filtration. Samples from relevant fractions were applied to SDS–PAGE and visualized by Coomassie blue staining.

Measuring 5-ALA synthesis rate

The 5-ALA synthesis rate was quantified as previously described (Goslings et al., 2004). CL-grown 16-d-old plants of WT, *flu*, *lsd1*, and *lsd1 flu* were vacuum-infiltrated for 5 min with an 80 mM LA (Sigma, St Louis, MO, USA) solution containing 10-mM KH_2PO_4 (pH 7.2) and 0.5% (v/v) Tween-20. After 1-h incubation at room temperature under CL, samples were immediately frozen in liquid nitrogen and then homogenized in 4% (v/v) TCA. The homogenates were lysed at 95°C for 15 min, cooled on ice for 2 min, and filtrated with 0.45-μm cellulose acetate membrane filters (Sterlitech, Auburn, Washington, USA). The filtrated lysates were neutralized with an equal volume of 0.5 M NaH_2PO_4 (pH 7.5). Afterward, ethylacetoacetate (1/5) was added and then the samples were incubated at 95°C for 10 min. After cooling on ice for 5 min, the extracts were mixed with the same volume of fresh Ehrlich's reagent [0.2 g *p*-dimethylaminobenzaldehyde (Sigma-Aldrich), 8.4-mL acetic acid, and 1.6-mL 70% (v/v) perchloric acid (Sigma-Aldrich)] and centrifuged at 14,000 *g* for 5 min at 4°C. The OD of each supernatant was measured at 553 nm using the NanoDrop 2000 (Thermo Fisher Scientific). The amount of 5-ALA was calculated using a coefficient of $7.45 \times 10^4\ mol^{-1}\ cm^{-1}$.

Determining photochemical efficiency

Measurements of photochemical efficiency of PSII (F_v/F_m) were conducted with a FluorCam system (FC800-C/1010GFP; Photon Systems Instruments) containing a CCD camera and an irradiation system according to the instrument manufacturer's instructions.

Trypan blue staining

Cell death was determined by trypan blue (TB) staining as described previously (Lv et al., 2019). The plant tissues were submerged in TB staining solution [25% (v/v) phenol, 25% (v/v) glycerol, 25% (v/v) lactic acid, 0.05% (w/v) TB] diluted with ethanol 1:2 (v/v) and boiled for 2 min. After incubating for 16 h on a vertical shaker at room temperature, the nonspecific staining was removed using destaining solution (250 g chloral hydrate dissolved in 100 mL H_2O, pH 1.2). Plant tissues were then kept in 50% (v/v) glycerol before taking images.

GO enrichment analysis

The RNA-seq data analyzed, as shown in Figure 3A, were previously published (Ni et al., 2017; Lv et al., 2019). The GO enrichment analysis of the selected genes, as shown in Supplemental Table S5, was performed on gprofiler (https://biit.cs.ut.ee/gprofiler) and represented the significantly enriched GO terms in the data set of BPs with a significance of $P < 0.05$.

Pigment analysis

The level of Pchlide was measured in 10-d-old plants of WT, *flu*, *lsd1*, and *lsd1 flu* as described by Goslings *et al.* (2004).

Accession numbers

Sequence information of the genes studied in this article can be found in the Arabidopsis TAIR database (https://www.arabidopsis.org) under the following accession numbers: *CAO* (At1g44446), *EX1* (At4g33630), *FLU* (At3g14110), *GLK1* (At2g20570), *GLK2* (At5g44190), *GUN4* (At3g59400), *GUN5* (At5g13630), *HEMA1* (At1g58290), *LHCA1* (At3g54890), *LHCB1.4* (At2g34430), *LHCB2.1* (At2g05100), *LHCB2.2* (At2g05070), *LHCB2.3* (At3g27690), *LHCB3* (At5g54270), *LHCB4.2* (At3g0890), *LHCB6* (At1g15820), *LSD1* (At4g20380), *PORA* (At5g54190), *PORB* (At4g27440), *PORC* (At1g03630), and *SIB1* (At3g56710).

Supplemental data

The following materials are available in the online version of this article.

Supplemental Figure S1. Detection of the LSD1–GFP fusion protein.

Supplemental Figure S2. Sequence alignment of Arabidopsis GLK1 and GLK2 proteins.

Supplemental Figure S3. Domain-deleted GLK1 and GLK2 variants localize to the nucleus.

Supplemental Figure S4. The C-terminal PRD region of GLKs is critical for LSD1–GLKs interaction.

Supplemental Figure S5. GO enrichment analysis toward the BP of the overlapped genes in Figure 3A.

Supplemental Figure S6. Expression levels of *GLK1* and *GLK2* in *oxLSD1* lines.

Supplemental Figure S7. LSD1 does not interact with SIB1 in vivo.

Supplemental Figure S8. SIB1 interacts with GLK1 through the N-terminal region of GLK1.

Supplemental Table S1. List of proteins obtained from LSD1 interactome analysis.

Supplemental Table S2. List of genes (91) overlapping between the *lsd1*-dependent upregulated genes (374) and *glk1 glk2*-dependent downregulated genes (936).

Supplemental Table S3. List of genes (395) upregulated in 17-d-old *lsd1* compared to WT.

Supplemental Table S4. List of genes (936) downregulated in *glk1 glk2* compared to WT.

Supplemental Table S5. GO term enrichment analysis of the 91 overlapping genes (shown in Supplemental Table S2) between the *lsd1*-dependent upregulated genes (395) and the *glk1 glk2*-dependent downregulated genes (936).

Supplemental Table S6. List of primer sets used in this study.

Acknowledgments

We thank the Core Facility of Proteomics in Shanghai Center for Plant Stress Biology for carrying out MS.

Funding

This research was supported by the Strategic Priority Research Program from the Chinese Academy of Sciences (Grant No. XDB27040102), the 100-Talent Program of the Chinese Academy of Sciences, and the National Natural Science Foundation of China (NSFC) (Grant No. 31871397) to C.K.

Conflict of interest statement. None declared.

References

Ahmad R, Liu Y, Wang TJ, Meng Q, Yin H, Wang X, Wu Y, Nan N, Liu B, Xu ZY (2019) GOLDEN2-LIKE transcription factors regulate WRKY40 expression in response to Abscisic acid. Plant Physiol **179:** 1844–1860

Apel K, Hirt H (2004) Reactive oxygen species: metabolism, oxidative stress, and signal transduction. Annu Rev Plant Biol **55:** 373–399

Aviv DH, Rusterucci C, Holt BF, 3rd, Dietrich RA, Parker JE, Dangl JL (2002) Runaway cell death, but not basal disease resistance, in lsd1 is SA- and NIM1/NPR1-dependent. Plant J **29**: 381–391

Beale SI, Castelfranco PA (1974) The biosynthesis of delta-aminolevulinic acid in higher plants: I. Accumulation of delta-aminolevulinic acid in greening plant tissues. Plant Physiol **53:** 291–296

Boruc J, Van den Daele H, Hollunder J, Rombauts S, Mylle E, Hilson P, Inze D, De Veylder L, Russinova E (2010) Functional modules in the Arabidopsis core cell cycle binary protein-protein interaction network. Plant Cell **22**: 1264–1280

Bravo-Garcia A, Yasumura Y, Langdale JA (2009) Specialization of the Golden2-like regulatory pathway during land plant evolution. New Phytol **183**: 133–141

Chai T, Zhou J, Liu J, Xing D (2015) LSD1 and HY5 antagonistically regulate red light induced-programmed cell death in Arabidopsis. Front Plant Sci **6:** 292

Chan KX, Phua SY, Crisp P, McQuinn R, Pogson BJ (2016) Learning the languages of the chloroplast: retrograde signaling and beyond. Annu Rev Plant Biol **67:** 25–53

Cheng J, He CX, Zhang ZW, Xu F, Zhang DW, Wang X, Yuan S, Lin HH (2011) Plastid signals confer Arabidopsis tolerance to water stress. Z Naturforsch C **66:** 47–54

Clough SJ, Bent AF (1998) Floral dip: a simplified method for *Agrobacterium*-mediated transformation of *Arabidopsis thaliana*. Plant J **16:** 735–743

Czarnocka W, Van Der Kelen K, Willems P, Szechynska-Hebda M, Shahnejat-Bushehri S, Balazadeh S, Rusaczonek A, Mueller-Roeber B, Van Breusegem F, Karpinski S (2017) The dual role of LESION SIMULATING DISEASE 1 as a condition-dependent scaffold protein and transcription regulator. Plant Cell Environ **40:** 2644–2662

Dietrich RA, Delaney TP, Uknes SJ, Ward ER, Ryals JA, Dangl JL (1994) Arabidopsis mutants simulating disease resistance response. Cell **77:** 565–577

Dietrich RA, Richberg MH, Schmidt R, Dean C, Dangl JL (1997) A novel zinc finger protein is encoded by the Arabidopsis LSD1 gene and functions as a negative regulator of plant cell death. Cell **88:** 685–694

Dogra V, Duan J, Lee KP, Lv S, Liu R, Kim C (2017) FtsH2-dependent proteolysis of EXECUTER1 is essential in mediating singlet oxygen-triggered retrograde signaling in *Arabidopsis thaliana*. Front Plant Sci **8:** 1145

Dogra V, Li M, Singh S, Li M, Kim C (2019) Oxidative post-translational modification of EXECUTER1 is required for singlet oxygen sensing in plastids. Nat Commun **10:** 2834

Dogra V, Rochaix JD, Kim C (2018) Singlet oxygen-triggered chloroplast-to-nucleus retrograde signalling pathways: an emerging perspective. Plant Cell Environ **41:** 1727–1738

Fitter DW, Martin DJ, Copley MJ, Scotland RW, Langdale JA (2002) GLK gene pairs regulate chloroplast development in diverse plant species. Plant J **31:** 713–727

Forreiter C, Apel K (1993) Light-independent and light-dependent protochlorophyllide-reducing activities and two distinct NADPH-protochlorophyllide oxidoreductase polypeptides in mountain pine (Pinus mugo). Planta **190**: 536–545

Goslings D, Meskauskiene R, Kim C, Lee KP, Nater M, Apel K (2004) Concurrent interactions of heme and FLU with Glu tRNA reductase (HEMA1), the target of metabolic feedback inhibition of tetrapyrrole biosynthesis, in dark- and light-grown Arabidopsis plants. Plant J **40:** 957–967

Han XY, Li PX, Zou LJ, Tan WR, Zheng T, Zhang DW, Lin HH (2016) GOLDEN2-LIKE transcription factors coordinate the tolerance to Cucumber mosaic virus in Arabidopsis. Biochem Biophys Res Commun **477:** 626–632

Hou Z, Yang Y, Hedtke B, Grimm B (2019) Fluorescence in blue light (FLU) is involved in inactivation and localization of glutamyl-tRNA reductase during light exposure. Plant J **97:** 517–529

Huang X, Li Y, Zhang X, Zuo J, Yang S (2010) The Arabidopsis LSD1 gene plays an important role in the regulation of low temperature-dependent cell death. New Phytol **187**: 301–312

Jabs T, Dietrich RA, Dangl JL (1996) Initiation of runaway cell death in an Arabidopsis mutant by extracellular superoxide. Science **273:** 1853–1856

Karpinski S, Szechynska-Hebda M, Wituszynska W, Burdiak P (2013) Light acclimation, retrograde signalling, cell death and immune defences in plants. Plant Cell Environ **36**: 736–744

Kim C, Meskauskiene R, Zhang S, Lee KP, Lakshmanan Ashok M, Blajecka K, Herrfurth C, Feussner I, Apel K (2012) Chloroplasts of Arabidopsis are the source and a primary target of a plant-specific programmed cell death signaling pathway. Plant Cell **24:** 3026–3039

Koussevitzky S, Nott A, Mockler TC, Hong F, Sachetto-Martins G, Surpin M, Lim J, Mittler R, Chory J (2007) Signals from chloroplasts converge to regulate nuclear gene expression. Science **316**: 715–719

Lai Z, Li Y, Wang F, Cheng Y, Fan B, Yu JQ, Chen Z (2011) Arabidopsis sigma factor binding proteins are activators of the WRKY33 transcription factor in plant defense. Plant Cell **23:** 3824–3841

Lee J, Choi B, Yun A, Son N, Ahn G, Cha JY, Kim WY, Hwang I (2021) Long-term abscisic acid promotes golden2-like1 degradation through constitutive photomorphogenic 1 in a light intensity-dependent manner to suppress chloroplast development. Plant Cell Environ **44:** 3034–3048

Lee JH, Jin S, Kim SY, Kim W, Ahn JH (2017) A fast, efficient chromatin immunoprecipitation method for studying protein-DNA binding in Arabidopsis mesophyll protoplasts. Plant Methods **13:** 42

Lee KP, Kim C, Landgraf F, Apel K (2007) EXECUTER1- and EXECUTER2-dependent transfer of stress-related signals from the plastid to the nucleus of *Arabidopsis thaliana*. Proc Natl Acad Sci USA **104:** 10270–10275

Lee KP, Liu K, Kim EY, Medina-Puche L, Dong H, Duan J, Li M, Dogra V, Li Y, Lv R, et al. (2020) PLANT NATRIURETIC PEPTIDE A and its putative receptor PNP-R2 antagonize salicylic acid-mediated signaling and cell death. Plant Cell **32:** 2237–2250

Li M, Kim C (2022) Chloroplast ROS and stress signaling. Plant Commun **3:** 100264

Li Z, Dogra V, Lee KP, Li R, Li M, Li M, Kim C (2020) N-terminal acetylation stabilizes SIGMA FACTOR BINDING PROTEIN1 involved in salicylic acid-primed cell death. Plant Physiol **183:** 358–370

Liu X, Li L, Li M, Su L, Lian S, Zhang B, Li X, Ge K, Li L (2018) AhGLK1 affects chlorophyll biosynthesis and photosynthesis in peanut leaves during recovery from drought. Sci Rep **8:** 2250

Livak KJ, Schmittgen TD (2001) Analysis of relative gene expression data using real-time quantitative PCR and the 2(-Delta Delta C(T)) Method. Methods **25**: 402–408

Lu Q, Tang X, Tian G, Wang F, Liu K, Nguyen V, Kohalmi SE, Keller WA, Tsang EW, Harada JJ, et al. (2010) Arabidopsis homolog of the yeast TREX-2 mRNA export complex: components and anchoring nucleoporin. Plant J **61:** 259–270

Lv R, Li Z, Li M, Dogra V, Lv S, Liu R, Lee KP, Kim C (2019) Uncoupled expression of nuclear and plastid photosynthesis-associated genes contributes to cell death in a lesion mimic mutant. Plant Cell **31**: 210–230

Martin G, Leivar P, Ludevid D, Tepperman JM, Quail PH, Monte E (2016) Phytochrome and retrograde signalling pathways converge to antagonistically regulate a light-induced transcriptional network. Nat Commun **7:** 11431

Meskauskiene R, Nater M, Goslings D, Kessler F, op den Camp R, Apel K (2001) FLU: a negative regulator of chlorophyll biosynthesis in *Arabidopsis thaliana*. Proc Natl Acad Sci USA **98:** 12826–12831

Miller G, Suzuki N, Rizhsky L, Hegie A, Koussevitzky S, Mittler R (2007) Double mutants deficient in cytosolic and thylakoid ascorbate peroxidase reveal a complex mode of interaction between reactive oxygen species, plant development, and response to abiotic stresses. Plant Physiol **144:** 1777–1785

Morikawa K, Shiina T, Murakami S, Toyoshima Y (2002) Novel nuclear-encoded proteins interacting with a plastid sigma factor, Sig1, in *Arabidopsis thaliana*. FEBS Lett **514:** 300–304

Muhlenbock P, Plaszczyca M, Plaszczyca M, Mellerowicz E, Karpinski S (2007) Lysigenous aerenchyma formation in Arabidopsis is controlled by LESION SIMULATING DISEASE1. Plant Cell **19:** 3819–3830

Muhlenbock P, Szechynska-Hebda M, Plaszczyca M, Baudo M, Mateo A, Mullineaux PM, Parker JE, Karpinska B, Karpinski S (2008) Chloroplast signaling and LESION SIMULATING DISEASE1 regulate crosstalk between light acclimation and immunity in Arabidopsis. Plant Cell **20**: 2339–2356

Murmu J, Wilton M, Allard G, Pandeya R, Desveaux D, Singh J, Subramaniam R (2014) Arabidopsis GOLDEN2-LIKE (GLK) transcription factors activate jasmonic acid (JA)-dependent disease susceptibility to the biotrophic pathogen Hyaloperonospora Arabidopsidis, as well as JA-independent plant immunity against the necrotrophic pathogen *Botrytis cinerea*. Mol Plant Pathol **15:** 174–184

Nagatoshi Y, Mitsuda N, Hayashi M, Inoue S, Okuma E, Kubo A, Murata Y, Seo M, Saji H, Kinoshita T, et al. (2016) GOLDEN 2-LIKE transcription factors for chloroplast development affect ozone tolerance through the regulation of stomatal movement. Proc Natl Acad Sci USA **113:** 4218–4223

Nandi DL, Shemin D (1968) Delta-aminolevulinic acid dehydratase of Rhodopseudomonas spheroides. 3. Mechanism of porphobilinogen synthesis. J Biol Chem **243:** 1236–1242

Ni F, Wu L, Wang Q, Hong J, Qi Y, Zhou X (2017) *Turnip Yellow Mosaic Virus* P69 interacts with and suppresses GLK transcription factors to cause pale-green symptoms in Arabidopsis. Mol Plant **10**: 764–766

Nott A, Jung HS, Koussevitzky S, Chory J (2006) Plastid-to-nucleus retrograde signaling. Annu Rev Plant Biol **57**: 739–759

Pogson BJ, Woo NS, Forster B, Small ID (2008) Plastid signalling to the nucleus and beyond. Trends Plant Sci **13**: 602–609

Rossini L, Cribb L, Martin DJ, Langdale JA (2001) The maize golden2 gene defines a novel class of transcriptional regulators in plants. Plant Cell **13:** 1231–1244

Rusaczonek A, Czarnocka W, Kacprzak S, Witon D, Slesak I, Szechynska-Hebda M, Gawronski P, Karpinski S (2015) Role of phytochromes A and B in the regulation of cell death and acclimatory responses to UV stress in *Arabidopsis thaliana*. J Exp Bot **66**: 6679–6695

Saraste M, Musacchio A (1994) Backwards and forwards binding. Nat Struct Biol **1**: 835–837

Savitch LV, Subramaniam R, Allard GC, Singh J (2007) The GLK1 'regulon' encodes disease defense related proteins and confers resistance to *Fusarium graminearum* in Arabidopsis. Biochem Biophys Res Commun **359**: 234–238

Shimizu T, Kacprzak SM, Mochizuki N, Nagatani A, Watanabe S, Shimada T, Tanaka K, Hayashi Y, Arai M, Leister D, et al. (2019) The retrograde signaling protein GUN1 regulates tetrapyrrole biosynthesis. Proc Natl Acad Sci USA **116:** 24900–24906

Siligardi G, Drake AF (1995) The importance of extended conformations and, in particular, the PII conformation for the molecular recognition of peptides. Biopolymers **37**: 281–292

Tadini L, Peracchio C, Trotta A, Colombo M, Mancini I, Jeran N, Costa A, Faoro F, Marsoni M, Vannini C, et al. (2020) GUN1 influences the accumulation of NEP-dependent transcripts and chloroplast protein import in Arabidopsis cotyledons upon perturbation of chloroplast protein homeostasis. Plant J **101:** 1198–1220

Tang H, Zhang D, Yuan S, Zhu F, Fu FQ, Wang S, Lin HH (2014) Plastid signals induce ALTERNATIVE OXIDASE expression to enhance the cold stress tolerance in *Arabidopsis thaliana*. Plant Growth Regul **74:** 275–283

Tang X, Miao M, Niu X, Zhang D, Cao X, Jin X, Zhu Y, Fan Y, Wang H, Liu Y, et al. (2016) Ubiquitin-conjugated degradation of golden 2-like transcription factor is mediated by CUL4-DDB1-based E3 ligase complex in tomato. New Phytol **209:** 1028–1039

Tokumaru M, Adachi F, Toda M, Ito-Inaba Y, Yazu F, Hirosawa Y, Sakakibara Y, Suiko M, Kakizaki T, Inaba T (2017) Ubiquitin-proteasome dependent regulation of the GOLDEN2-LIKE 1 transcription factor in response to plastid signals. Plant Physiol **173:** 524–535

Tzfira T, Tian GW, Lacroix B, Vyas S, Li J, Leitner-Dagan Y, Krichevsky A, Taylor T, Vainstein A, Citovsky V (2005) pSAT vectors: a modular series of plasmids for autofluorescent protein tagging and expression of multiple genes in plants. Plant Mol Biol **57:** 503–516

Wagner D, Przybyla D, Op den Camp R, Kim C, Landgraf F, Lee KP, Wursch M, Laloi C, Nater M, Hideg E, et al. (2004) The genetic basis of singlet oxygen-induced stress responses of *Arabidopsis thaliana*. Science **306:** 1183–1185

Waters MT, Moylan EC, Langdale JA (2008) GLK transcription factors regulate chloroplast development in a cell-autonomous manner. Plant J **56:** 432–444

Waters MT, Wang P, Korkaric M, Capper RG, Saunders NJ, Langdale JA (2009) GLK transcription factors coordinate expression of the photosynthetic apparatus in Arabidopsis. Plant Cell **21:** 1109–1128

Wu GZ, Meyer EH, Richter AS, Schuster M, Ling Q, Schottler MA, Walther D, Zoschke R, Grimm B, Jarvis RP, et al. (2019) Control of retrograde signalling by protein import and cytosolic folding stress. Nat Plants **5**: 525–538

Xie YD, Li W, Guo D, Dong J, Zhang Q, Fu Y, Ren D, Peng M, Xia Y (2010) The Arabidopsis gene SIGMA FACTOR-BINDING PROTEIN 1 plays a role in the salicylate- and jasmonate-mediated defence responses. Plant Cell Environ **33:** 828–839

Yoo SD, Cho YH, Sheen J (2007) Arabidopsis mesophyll protoplasts: a versatile cell system for transient gene expression analysis. Nat Protoc **2**: 1565–1572

Zarrinpar A, Bhattacharyya RP, Lim WA (2003) The structure and function of proline recognition domains. Sci STKE **2003:** RE8

Zhang D, Tan W, Yang F, Han Q, Deng X, Guo H, Liu B, Yin Y, Lin H (2021a) A BIN2-GLK1 signaling module integrates brassinosteroid and light signaling to repress chloroplast development in the dark. Dev Cell **56**: 310–324e317

Zhang H, Zhang L, Ji Y, Jing Y, Li L, Chen Y, Wang R, Zhang H, Yu D, Chen L (2021b) Arabidopsis SIGMA FACTOR BINDING PROTEINs function antagonistically to WRKY75 in abscisic acid-mediated leaf senescence and seed germination. J Exp Bot erab391

Zhang ZW, Feng LY, Cheng J, Tang H, Xu F, Zhu F, Zhao ZY, Yuan M, Chen YE, Wang JH, et al. (2013) The roles of two transcription factors, ABI4 and CBFA, in ABA and plastid signalling and stress responses. Plant Mol Biol **83**: 445–458

Zhang ZW, Yuan S, Xu F, Yang H, Chen YE, Yuan M, Xu MY, Xue LW, Xu XC, Lin HH (2011) Mg-protoporphyrin, haem and sugar signals double cellular total RNA against herbicide and high-light-derived oxidative stress. Plant Cell Environ **34:** 1031–1042

Zhao X, Huang J, Chory J (2019) GUN1 interacts with MORF2 to regulate plastid RNA editing during retrograde signaling. Proc Natl Acad Sci USA **116:** 10162–10167